bioRxiv preprint doi: https://doi.org/10.1101/2021.10.25.465674; this version posted October 26, 2021. The copyright holder for this preprint (which was not certified by peer review) is the author/funder. All rights reserved. No reuse allowed without permission.

MeDUsA: A novel system for automated axon quantification to evaluate neuroaxonal degeneration

Yohei Nitta[1*], Hiroki Kawai[2*], Jiro Osaka[3], Satoko Hakeda-Suzuki[3], Yoshitaka Nagai[4, 5], Karolína Doubková[6,7], Takashi Suzuki[3], Gaia Tavosanis[6,7], Atsushi Sugie[1]

1. Brain Research Institute, Niigata University, Niigata, Japan
2. LPIXEL Inc., Tokyo, Japan
3. School of Life Science and Technology, Tokyo Institute of Technology, Yokohama, Japan
4. Department of Neurotherapeutics, Osaka University Graduate School of Medicine, Suita, Japan
5. Department of Neurology, Kindai University Faculty of Medicine, Osaka-Sayama, Japan
6. German Center for Neurodegenerative Diseases (DZNE), Bonn, Germany
7. LIMES Institute, University of Bonn, Germany

* Equal contribution

Corresponding author: atsushi.sugie@bri.niigata-u.ac.jp (A.S.).

Abstract:

Background: *Drosophila* is an excellent model organism for studying human neurodegenerative diseases (NDs), and the rough eye phenotype (REP) assay is a

bioRxiv preprint doi: https://doi.org/10.1101/2021.10.25.465674; this version posted October 26, 2021. The copyright holder for this preprint (which was not certified by peer review) is the author/funder. All rights reserved. No reuse allowed without permission.

convenient experimental system for analysing the toxicity of ectopically expressed human disease genes. However, the association between REP and axonal degeneration, an early sign of ND, remains unclear. To address this question, we developed a method to evaluate axonal degeneration by quantifying the number of retinal R7 axons in *Drosophila*; however, it requires expertise and is time-consuming. Therefore, there is a need for an easy-to-use software that can automatically quantify the axonal degeneration.

Result: We created MeDUsA (a 'method for the quantification of degeneration using fly axons'), which is a standalone executable computer program based on Python that combines a pre-trained deep-learning masking tool with an axon terminal counting tool. This software automatically quantifies the number of axons from a confocal z-stack image series. Using this software, we have demonstrated for the first time directly that axons degenerate when the causative factors of NDs (αSyn, Tau, TDP-43, HTT) were expressed in the *Drosophila* eye. Furthermore, we compared axonal toxicity of the representative causative genes of NDs and their pathological alleles with REP and found no significant correlation between them.

Conclusions: MeDUsA rapidly and accurately quantifies axons in *Drosophila* eye. By simplifying and automating time-consuming manual efforts requiring significant expertise, it enables large-scale, complex research efforts on axonal degeneration, such as screening to identify genes or drugs that mediate axonal toxicity caused by ND disease proteins.

Keywords:

Axonal degeneration, Quantification, Standalone program, *Drosophila*, Neurodegenerative disease

bioRxiv preprint doi: https://doi.org/10.1101/2021.10.25.465674; this version posted October 26, 2021. The copyright holder for this preprint (which was not certified by peer review) is the author/funder. All rights reserved. No reuse allowed without permission.

49

50 **Background:**

51 Neurodegenerative diseases (NDs) are disorders in which certain groups of neurons in
52 the brain and spinal cord involved in cognitive and motor function are gradually lost.
53 Molecular genetic studies have identified causative genes and risk factors and elucidated
54 the mechanisms of pathogenesis at the molecular level. These findings revealed that
55 structural defects and aggregation of disease-associated proteins underlie
56 neurodegenerative processes [1]. It has become available to examine the effects of novel
57 mutations found in human diseases like NDs, whether they result in the loss of gene
58 function or gain of toxic function, using various model organisms. Among them,
59 *Drosophila* has various advantages as a neuronal disease model. For example, 1) gene
60 function can be analysed without strongly considering the compensation of gene function
61 by duplication since there are relatively few duplicated genes in the genome; 2) research
62 sample sizes can be large because individuals are small, inexpensive and easy to breed;
63 3) the short life cycle allows rapid genetic analysis and 4) the organism has a compact
64 brain, making it possible to analyse at the level of neural circuitry and behaviour
65 necessary for higher functions such as learning, memory and sleep. Taking advantage of
66 these features, *Drosophila* is widely used in studies on human diseases. Further, it has
67 been reported that the expression of a human disease-associated protein in *Drosophila*
68 induces toxicity even in flies [2–6], demonstrating the conservation of molecular
69 mechanisms between humans and flies.

70 Trinucleotide repeat disorders are human diseases caused by the expansion of
71 CAG repeats in the protein-coding regions of causative genes. Spinocerebellar ataxia type
72 3 (SCA3), also known as Machado-Joseph disease, is a neurodegenerative disease caused

bioRxiv preprint doi: https://doi.org/10.1101/2021.10.25.465674; this version posted October 26, 2021. The copyright holder for this preprint (which was not certified by peer review) is the author/funder. All rights reserved. No reuse allowed without permission.

by repeated elongation of glutamine. In *Drosophila*, the expression of these extended polyglutamine repeats not only formed inclusion bodies similar to those in humans, but also caused degeneration [2]. CAG repeats are also found in Huntingtin (HTT), the gene responsible for Huntington's disease, which is another autosomal dominant neurodegenerative disease. In experiments in which polyglutamine-extended HTT was expressed in the photoreceptors of *Drosophila*, inclusion bodies formed and the polyglutamine-extended HTT induced neurodegeneration [3]. Additionally, in Parkinson's disease (PD), a neurodegenerative disorder characterised by the loss of dopaminergic neurons in the substantia nigra, formation of Lewy bodies and impaired motility, expression of the causative gene synuclein alpha (SNCA) in *Drosophila* caused the loss of dopaminergic neurons, the formation of fibrous intraneuronal inclusions containing Alpha-synuclein (αSyn) and motor dysfunction [4]. Furthermore, the expression of the microtubule-associated protein Tau, which is involved in Alzheimer's disease, in all neurons of *Drosophila* led to the observation of progressive neurodegeneration [5]. Thus, *Drosophila* models expressing human disease-causing genes can reproduce the characteristics of human diseases, thereby enabling powerful genetic approaches to study various NDs such as polyglutamine disease, synucleinopathy and tauopathy. Using these ND models, large genetic screens can be performed to explore unknown protein networks in which disease-causing proteins interact. The homologues of the candidate network members can then be identified in the human genome to determine whether they are susceptibility genes of the disease of interest. In one example of a disease study of amyotrophic lateral sclerosis (ALS), genetic screening using this experimental paradigm identified that ATXN2 is involved in ALS pathogenesis [7]. Further, suppression of the ATXN2 *Drosophila* homologue reduced the toxicity of

bioRxiv preprint doi: https://doi.org/10.1101/2021.10.25.465674; this version posted October 26, 2021. The copyright holder for this preprint (which was not certified by peer review) is the author/funder. All rights reserved. No reuse allowed without permission.

97 TDP-43, which is a DNA/RNA-binding protein implicated in several NDs. The discovery
98 of ATXN2 accumulation in the spinal cord of human ALS is but one example revealed
99 using this screening approach in *Drosophila*.

100 The rough eye phenotype (REP), which is frequently used to investigate genetic
101 interactions in *Drosophila*, is also used in disease research as a convenient and quick way
102 to assess the toxicity of ectopically expressed genes. The phenotypic assay uses the
103 Gal4/UAS method [8] to evaluate the toxicity of a gene of interest by expressing it
104 specifically in the eye using the eye-specific *Gal4*, *GMR-Gal4* and observing eye
105 structure. In fact, this fly eye assay has identified several modifiers that inhibit or enhance
106 the toxicity caused by pathogenic factors such as Tau [9–11], αSyn [12–15], TDP-43
107 [16,17] and polyglutamated HTT [18–20]. Moreover, drug screenings can be performed
108 by adding compounds to fly food, and compounds that reduce disease toxicity can be
109 identified [21,22]. Although REP has been evaluated qualitatively in most previous
110 studies, several research groups have recently reported methods for the quantitative
111 evaluation of REP [23,24]. However, it remains unclear whether REP reflects
112 neurodegeneration completely as the formation and geometric defects of cell clusters are
113 assessed only within the ommatidium, which contains cone and pigment cells. To assess
114 neurodegeneration more fully in *Drosophila*, several other parameters related to
115 neurodegeneration, as measured by protein aggregation number, vacuolar size and
116 number and retinal thickness, have been previously developed [25]. However, these
117 systems also indirectly observe neurodegeneration, and therefore, a direct quantitative
118 method for accurately measuring neurodegeneration is required.

119 Axonal degeneration is a representative pathology of neurodegeneration, and
120 the magnitude of neurodegeneration can be accurately evaluated by its quantification. To

bioRxiv preprint doi: https://doi.org/10.1101/2021.10.25.465674; this version posted October 26, 2021. The copyright holder for this preprint (which was not certified by peer review) is the author/funder. All rights reserved. No reuse allowed without permission.

date, there are few methods for quantifying axonal degeneration [26,27]. Further, they are time-consuming, requiring the manual quantification of axonal number or depend on the expertise of experimenters to accurately classify the degree of degeneration. However, biological images contain noise, and variable signal intensities are often observed among samples. Additionally, the three-dimensional (3D) structure and angle are never uniform between images. Thus, to recognise the semantic region from diverse image data, the eye of a trained researcher can flexibly and accurately extract specific phenomena to be analysed, but such time-consuming methods are not suitable for screening to identify genes or compounds that modify the pathology and requires quantifying large numbers of samples. Therefore, robust image processing systems other than the human eye are required to evaluate axonal degeneration simply and quickly. In recent years, image processing technology has made remarkable progress, especially the development of deep-learning technology using convolutional neural networks (CNNs), which has greatly advanced the field of image recognition, and is also true in the field of biological images [28]. In addition, although conventional image processing can extract signal regions, it is difficult to extract semantic regions, but CNN has demonstrated high performance in semantic domain segmentation. In particular, U-Net [29] is an architecture of CNNs designed for biological image analysis, and U-Net and its derived architectures have been used for segmentation tasks in the area of biological image analysis with great success [30–33].

In an accompanying study, we developed a novel method to directly quantify axonal degeneration using R7, a photoreceptor neuron type in *Drosophila*, as a model [34]. In this method, axon terminals are manually excised from the confocal microscope z-stack image series, and degeneration is quantified by manual counting the number of

bioRxiv preprint doi: https://doi.org/10.1101/2021.10.25.465674; this version posted October 26, 2021. The copyright holder for this preprint (which was not certified by peer review) is the author/funder. All rights reserved. No reuse allowed without permission.

145 axon terminals. This allowed quantifying even minor axon losses; therefore, even very
146 early stages of axonal degeneration phenomena. Nonetheless, its throughput was not
147 sufficient for larger scale screens. To automate the method, we established here a novel
148 software package called 'method for the quantification of degeneration using fly axons'
149 (MeDUsA) by combining deep learning with a Python-based counting system. Using this
150 software, we assessed the effects on axons among the causative genes of several NDs and
151 found that they exhibited axonal degeneration. Additionally, no significant correlation
152 was detected between the number of axons and the REP. MeDUsA provides direct and
153 rapid quantitation of axonal degeneration in *Drosophila*, making it a powerful tool that
154 can be used in disease and developmental studies.
155
156 **Results:**
157 **Rough eye phenotype is insufficient to speculate on gene effects in axonal**
158 **degeneration**
159 The Rough eye phenotype (REP) assay has been extensively used to study
160 neurodegenerations (NDs) [35]; however, there is uncertainty whether REP accurately
161 reflects axonal degeneration. We performed a modifier genetic screening designed to
162 identify genes that modulate the toxicity of TDP-43 by observing retinal and axonal
163 degeneration phenotypes. The *Drosophila* photoreceptors R7 and R8 project their axons
164 directly from the compound eye retina through the primary optic ganglion lamina to the
165 secondary optic ganglion medulla (Fig. 1A). For this screening, a fly line with eye-
166 specific expression of TDP-43^{G298S}, which is an ALS-associated mutation of TDP-43 [36],
167 using *GMR-Gal4* [37,38] was generated. These flies were crossed with 99 candidate RNA
168 interference (RNAi) lines (Fig. 1B; see Materials and Methods). In the first screening

bioRxiv preprint doi: https://doi.org/10.1101/2021.10.25.465674; this version posted October 26, 2021. The copyright holder for this preprint (which was not certified by peer review) is the author/funder. All rights reserved. No reuse allowed without permission.

round, we observed the eye phenotype because the eye-specific expression of TDP-43^{G298S} causes REP as previously reported [39]. As a result, 14 of 99 RNAi lines were identified that suppress REPs (Fig. 1B, 1C). Next, we evaluated the axonal degeneration of R8 retinal axons, as the second screening round (Fig. 1B, 1C). To quantify the axonal degeneration, we calculated the ratio of degenerated axons in the part of the optic lobe that is easy to observe each axon. We classified an axon as degenerated when the axon was fragmented. Eye-specific expression of TDP-43 displayed axonal degeneration of R8 axons one day after eclosion (Fig. 1C). We expected that REPs identified in the first screening round would be consistent with the morphology of the R8 axons under the assumption that RNAi lines which suppressed REPs rescued the axonal degeneration. Surprisingly, the REP results did not always match those of axonal degeneration. Knockdown of *Dsk*, a neuropeptide-encoding gene identified in only crustaceans and insects, in the background of TDP-43 expression strongly suppressed REP; however, *Dsk* knockdown significantly promoted axonal degeneration (Fig. 1C; quantified in 1D). In addition, the knockdown of 10 genes did not affect axonal degeneration, whereas 3 genes (*mle*, *faf* and *caz*) rescued the degeneration (Fig. 1C; quantified in 1D). Thus, although the REP assay is a simple and powerful method for assessing toxicity, it is insufficient to evaluate axonal degeneration. Further, the quantitative method we used to assess degeneration in this screening was also insufficient for precise quantification because it was a subjective determination whether an axon was degenerated (i.e. fragmented) or intact. Other limitations include the fact that axons which are completely lost cannot be counted and all R8 axons were not counted from the dorsal view due to limits of the confocal microscope scanning time and depth at which the sample could be viewed cleanly. Additionally, depending on the person performing the method and region being

bioRxiv preprint doi: https://doi.org/10.1101/2021.10.25.465674; this version posted October 26, 2021. The copyright holder for this preprint (which was not certified by peer review) is the author/funder. All rights reserved. No reuse allowed without permission.

quantified, the results would display a high degree of variability. Therefore, we developed an automatic system, MeDUsA for the unbiased quantitative evaluation of axonal degeneration in *Drosophila*.

The process flow for using MeDUsA

To quantify R7 axons using MeDUsA, the first step is to prepare samples of the *Drosophila* brain (Fig. 2A and 2B). Dissection and immunostaining were performed as previously described [34,40] .

In the second step, axon termini were identified and quantified. For this purpose, we developed MeDUsA to enable non-experts to accurately evaluate axonal degeneration and to save time. MeDUsA utilises a combination of tools available in Python that allows the task of masking axons to be performed by pre-trained deep learning, followed by automatic counting of axon terminals after masking. This software enables researchers to quantify the number of R7 axons readily and quickly, taking 50 seconds per sample on a general desktop workstation (CPU: Intel Core i7 9800X 3.8 GHz, RAM: DDR4 128 GB).

To create a model that generates a mask of the surface area, we trained a 2D-U-Net architecture (Fig. 2C). However, to determine the surface area, it is necessary to infer it from the axon terminal signals in the sparsity, and there are areas where it is difficult to determine the surface area with a single z-slice. Therefore, we trained the 2D-U-Net to generate a surface mask of three slices by inputting three slices as three channels, including the slice before and after the slice of interest. Then, during inference, only the mask of the centre slice was used. The training and testing datasets included both normal and abnormal images. A total of 16,114 images in 199 samples were used for training and

bioRxiv preprint doi: https://doi.org/10.1101/2021.10.25.465674; this version posted October 26, 2021. The copyright holder for this preprint (which was not certified by peer review) is the author/funder. All rights reserved. No reuse allowed without permission.

1,375 images in 16 samples were used for testing. By using three channels, the dice score improved from 0.815 to 0.847 compared to using a single channel.

After mask generation and axon terminal extraction, the number of axonal terminals was counted automatically (Fig. 2D). To do this, we first filtered the regional maxima to remove background, followed by binarisation using adaptive thresholding. The surface area was then extracted using mask images. We performed a Euclidean distance transformation to obtain peaks, which were used as seeds to perform 3D watershed to obtain each axon terminal candidate. Finally, candidates below 20 voxels (equivalent to a radius of about 1.68 μm) were eliminated, and the remaining ones were counted as axon terminals. This process was fully automated and allowed us to stably detect axon terminals without adjusting parameters for each sample.

Ectopic expression of causative genes of NDs causes axonal degeneration in R7 neurons

Using our MeDUsA, we evaluated the effect of mutations in proteins responsible for NDs on axonal degeneration in *Drosophila*. We expressed either wild-type or well-known mutant alleles of human causative genes for neurodegenerative diseases (αSyn, Tau, TDP-43 and HTT) in photoreceptor axons using *GMR-Gal4* and predicted the number of axonal terminals in 1-day-old adults. The ectopic expression of wild-type αSyn, which is a causative gene of PD [41], in photoreceptor axons did not show a significant reduction in axonal number compared to control, whereas the expression of A53T-mutated αSyn, a well-known pathogenic allele associated with familial PD [42], caused a significant reduction in the number of axons compared to control (Fig. 3A–C; quantified in 3K). However, there was no significance between wild-type and A53T-mutated αSyn. Next,

bioRxiv preprint doi: https://doi.org/10.1101/2021.10.25.465674; this version posted October 26, 2021. The copyright holder for this preprint (which was not certified by peer review) is the author/funder. All rights reserved. No reuse allowed without permission.

we found that expression of wild-type Tau (Tau^{WT}), which is implicated in Alzheimer's disease, caused significant axonal degeneration, and the expression of Tau with the R406W mutation, which is a missense mutation identified in families diagnosed with frontotemporal dementia and parkinsonism linked to chromosome 17 [43], enhanced the degeneration (Fig. 3D, 3E; quantified in 3K). Interestingly, the expression of Tau with the S2A mutation, a mutation with impaired phosphorylation capabilities, significantly suppressed axonal degeneration compared to Tau^{WT} (Fig. 3F), indicating that phosphorylated Tau exhibits toxicity. Next, we evaluated the expression of both wild-type and A315T-mutated [44] TDP-43, which has been identified as the major disease protein in ALS, in photoreceptor axons, and found that both displayed axonal degeneration, although degeneration was milder in the A315T mutant than in wild-type TDP-43 (Fig. 3G, 3H; quantified in 3K). Finally, we found that ectopic expression of wild-type HTT (HTT^{Q0}), the causative gene of Huntington's disease, did not cause axonal degeneration, whereas the expression of HTT with a pathogenic polyQ tract of 128 repeats (HTT^{Q128}) significantly reduced the number of R7 axons (Fig. 3I, 3J; quantified in 3K). These results show that the ectopic expression of causative genes of human NDs induced axonal degeneration in *Drosophila*, and well-known pathogenic mutations enhanced degeneration, except for TDP-43. Our findings demonstrate that the toxicity of various human disease causative proteins can be reliably assessed across species using our quantitative axonal degeneration fly model.

To evaluate the performance of MeDUsA, we quantified the axonal number of the same sample set manually (Fig. 4A). This manual method enabled us to carry out precise quantification of axonal number; however, manual quantification is time-consuming and several parameters have to be adjusted for each sample to detect axon

bioRxiv preprint doi: https://doi.org/10.1101/2021.10.25.465674; this version posted October 26, 2021. The copyright holder for this preprint (which was not certified by peer review) is the author/funder. All rights reserved. No reuse allowed without permission.

terminals. The MeDUsA measurements were lower than the manual measurements (Fig. 4B). This is due to the severity of the setting (Fig. 2D) for recognising the axon terminal in automated quantification. If the setting is further set loose, the false positive count increases. At present, this is the limitation of the MeDUsA. Nevertheless, the system showed a quadratic weighted kappa score (κ2) of 0.724 and a significantly strong positive correlation with manual counting (individual values, $R^2 = 0.887$, $p < 0.001$, Fig. 4C; mean value per genotype, $R^2 = 0.944$, $p < 0.001$, Fig. 4D). Taken together, these findings demonstrate that MeDUsA automatically and rapidly counts axonal number in a preparation accessible for genetic screening.

REP does not match the axonal degeneration phenotype

Next, we evaluated the correlation between axonal degeneration phenotype and the REP. To quantify REP severity, we used Flynotyper that calculates the phenotypic score from the disarray of the ommatidia [24]. We expressed the same set of causative genes for NDs in the eye using *GMR-Gal4* as in axonal degeneration experiments and quantified the degree of phenotypic severity of eye phenotypes in 1-day-old adults. We found that the expression of either the wild-type or pathogenic allele of αSyn did not significantly increase the phenotypic score compared to control (Fig. 5A–C; quantified in 5K), although the expression of the pathogenic alleles of αSyn caused axonal degeneration (Fig. 3K). In contrast, REP severity was consistent with the reduction of axonal number when the wild-type and mutant alleles of Tau were expressed (Fig. 5D–F; quantified in 5K). Wild-type and R406W-mutated Tau, both of which caused axonal degeneration, showed a significantly increased phenotypic score, whereas the S2A mutation did not display any reduction in axonal number nor corresponding score increase. Similar to αSyn,

bioRxiv preprint doi: https://doi.org/10.1101/2021.10.25.465674; this version posted October 26, 2021. The copyright holder for this preprint (which was not certified by peer review) is the author/funder. All rights reserved. No reuse allowed without permission.

we found that TDP-43 expression showed an obvious discrepancy between the two phenotypes. As described earlier, wild-type TDP-43 is more toxic than A315T-mutated TDP-43 on axonal degeneration (Fig. 3K). However, the A315T mutation caused a significant increase in the REP score compared with wild-type TDP-43 (Fig. 5G, 5H; quantified in 5K). HTT expression also exhibited differences between axon and eye phenotypes. In contrast to axonal degeneration phenotypes, the ectopic expression of HTT^{Q128} did not cause REPs (Fig. 5I, 5J; quantified in 5K). Finally, we determined the correlation between the average axonal number and average phenotypic score of rough eye in each genotype, and found a negative correlation, but the correlation was not statistically significant ($R = -0.467$, $p = 0.174$). Taken together, our findings show that REP scoring is not exactly consistent with the degree of axonal degeneration.

Discussion:

We recently developed a method that precisely quantifies the axonal number of retinal R7 neurons by creating a mask which extracts the axon terminals [34]. In the present study, we developed and tested MeDUsA, a software that automatically creates masks and counts axon terminals using a combination of deep learning and Python (Fig. 2). By using this software, the number of R7 axons can be automatically quantified easily and quickly from confocal images. Conventionally, REP is frequently used to assess neurotoxicity in fly studies because it does not require special equipment and can be readily performed; however, we found that the severity of REP is not always consistent with axonal toxicity (Fig. 3 and Fig. 5). Also conditions that induce sporadic progressive axonal degeneration of R7 are not accompanied by cell death [34]. Therefore, we propose that ND research can be conducted more efficiently by combining REP with our method

bioRxiv preprint doi: https://doi.org/10.1101/2021.10.25.465674; this version posted October 26, 2021. The copyright holder for this preprint (which was not certified by peer review) is the author/funder. All rights reserved. No reuse allowed without permission.

when the focus is axonal degeneration. Although several models for evaluating axonal degeneration in *Drosophila* have been reported [26,27,34], they are technically difficult and exceedingly time-consuming to evaluate axonal degeneration in large-scale experiments such as screening as the evaluation of degeneration in these models is subjective or require manual measurement. However, by using MeDUsA, it is not only possible to identify factors and chemical compounds that inhibit axonal degeneration in the fly model of ND by screening but also to easily evaluate axonal toxicity of new or undiagnosed variants of pathological proteins of ND.

According to our modifier screening using REP to identify genes that suppress TDP-43^{G298S} toxicity, we identified 14 candidate genes. Further investigation focused on axonal degeneration showed that the knockdown of three genes (*mle*, *caz* and *faf*) suppressed toxicity, whereas *Dsk* knockdown promoted it (Fig. 1C, 1D). *Dsk* encodes the cholecystokinin-like neuropeptide Drosulfakinin and has been reported to be involved in feeding behaviour, aggression and larval avoidance [45–48]. A previous study reported that Dsk is also involved in synaptogenesis in the neuromuscular junction in cooperation with a putative cholecystokinin-like receptor [49]. Studies in mouse models have shown that the pathogenic form of TDP-43 has harmful effects on synapses. For example, hyperexcitability has been observed [50] and spine density has been reduced [51]. Therefore, our results suggest that Dsk reduction causes synapse dysfunction and make axons fragile, whereby axonotoxicity of TDP-43^{G298S} is enhanced. Named by its male-specific lethal phenotype in loss-of-function mutants, *mle* (*maleless*) encodes an RNA helicase and is a member of the Male-Specific-Lethal transcription complex, which is involved in dosage compensation in males [52]. The homologue of *mle* in human, *DHX9*, was reported to encode a TDP-43–interacting protein [53]. Furthermore, a previous study

bioRxiv preprint doi: https://doi.org/10.1101/2021.10.25.465674; this version posted October 26, 2021. The copyright holder for this preprint (which was not certified by peer review) is the author/funder. All rights reserved. No reuse allowed without permission.

reported in a fly model that knockdown of *mle* exacerbated neurodegeneration caused by the expression of expanded UGGAA, which is considered responsible for spinocerebellar ataxia type 31 (SCA31), whereas overexpression of wild-type TDP-43 suppressed expanded UGGAA-induced toxicity [39]. Thus, *mle* may be involved in the RNA-dependent toxicity of TDP-43. *caz* (*cabeza*), which encodes a RNA-binding protein, is a fly homologue of FUS/TLS, which is another major causative gene for ALS. Physical interactions between human FUS/TLS and TDP-43 have been reported in mammalian cultured cells [54,55], and it has been suggested that FUS/TLS is genetically located downstream of TDP-43 in fly and fish models [56,57]. Therefore, the attenuation of axonal degeneration by *caz* knockdown may be due to the suppression of excess unknown downstream factors of TDP-43 or *caz* itself or both. The influence of *faf* (fat facets), which encodes a deubiquitylated enzyme and is a fly homologue of *USP9X*, on neurodegeneration varies among fly ND models. Lee et al. reported that FAF enhanced the toxicity of amyloid precursor protein (APP) and Aβ-42. The co-expression of FAF with either APP or Aβ-42 enhanced REP and knockdown of *faf* suppressed the post-synaptic toxicity of APP and Aβ-42 [58]. Another group revealed that reduced levels of *faf* enhanced retinal toxicity of HTT [19]. As FAF deubiquitinates different substrates in these diseases, it may be reflected in the different effects on the toxicity of causative proteins of the ND. Further analysis of these genes would shed light on the molecular mechanisms underlying axonotoxicity by TDP-43^{G298S}.

Using the automatic quantification method developed in this study, we evaluated the axonal effects of several representative causative factors of NDs, including αSyn, Tau, TDP-43 and HTT (Fig. 3). Although the pathological significance of these causal factors has been examined in various model organisms, including fly model, few

bioRxiv preprint doi: https://doi.org/10.1101/2021.10.25.465674; this version posted October 26, 2021. The copyright holder for this preprint (which was not certified by peer review) is the author/funder. All rights reserved. No reuse allowed without permission.

360 studies have directly visualised and quantitatively evaluated axonal degeneration such as
361 that demonstrated in this study using MeDUsA. Our findings show that MeDUsA is
362 highly extensible and can be used in different NDs to demonstrate how a causative gene
363 affects axonal degeneration.

364 *SNCA* encodes αSyn, which is highly localised at the pre-synaptic terminal, and
365 is thought to mediate the regulation of synaptic function [59]. Studies using post-mortem
366 brains and primary neurons from patients with PD suggest that αSyn aggregates in axons
367 and causes degeneration, resulting in impaired neuronal function that is propagated to the
368 cell body and leads to neuronal death [60,61]. The A53T mutation is a well-known toxic
369 mutation of αSyn that aggregates more rapidly and forms fibrils than wild-type, and many
370 studies using animal models and induced pluripotent stem (iPS) cells derived from
371 patients with PD have reported high neurotoxicity [62–64]. In our study, a significant
372 reduction in the number of axons was observed between control and αSyn^{A53T}-expressed
373 flies, but no statistically significant difference was observed between wild-type and A53T
374 (Fig. 3K). A possible reason for the non-significant difference is that quantification was
375 performed too early (1-day-old adult), and differences between the wild-type and A53T
376 mutation may be observed if quantified several weeks after eclosion.

377 Tau is a microtubule-associated protein that binds to microtubules and
378 maintains their stability in neurons. In tauopathies, Tau is thought to be dissociated from
379 microtubules by excessive phosphorylation and aggregate, causing a dying-back pattern
380 of neurodegeneration [65]. Although several studies have reported increased toxicity with
381 the R406W mutation, a change in the phosphorylation status remains controversial.
382 Studies using *in vitro* and patient-derived iPS cells have reported that R406W mutant *tau*
383 is less phosphorylated than wild-type *tau*, whereas excessive phosphorylation has been

bioRxiv preprint doi: https://doi.org/10.1101/2021.10.25.465674; this version posted October 26, 2021. The copyright holder for this preprint (which was not certified by peer review) is the author/funder. All rights reserved. No reuse allowed without permission.

384 observed in both murine model and post-mortem patient brain [66–69]. Although
385 previous studies reported that overexpression of Tau^{R406W}, which was used in this study,
386 displayed high toxicity in REP compared to Tau^{WT} in *Drosophila* [5,70], it may be due
387 to positional effects of the UAS insertion site [71]. Consistent with previous reports, we
388 found that Tau^{R406W} overexpression exerted a more toxic effect on axons than Tau^{WT}
389 overexpression (Fig. 3K).

390 TDP-43 is a highly conserved 43 kDa RNA-binding protein that is a main
391 component of ubiquitinated aggregation in the neurons of patients with ALS and
392 frontotemporal lobar degeneration (FTLD) [72]. Numerous studies that have investigated
393 the physiological function of TDP-43 have revealed that TDP-43 is involved in various
394 aspects of RNA metabolism, and these disturbances may be responsible for the
395 pathogenesis of ALS and FTLD [73]. In many model organisms, both overexpression and
396 loss-of-function of TDP-43 result in reduced longevity and motor function [74–77]. The
397 overexpression of wild-type TDP-43 in *Drosophila* mushroom body neurons of the
398 olfactory memory centre causes axonal degeneration [78], whereas the effects of the
399 A315T mutation on TDP-43 toxicity are controversial in *Drosophila*. Guo et al. reported
400 that TDP-43^{A315T} was more toxic to motor neurons than TDP-43^{WT}, whereas Patricia et
401 al. reported that TDP-43^{WT} showed severe toxicity compared to TDP-43^{A315T}, except for
402 larval locomotor activity [79,80]. In our present result of retinal R7 axons, we found that
403 wild-type TDP-43 showed higher axonal toxicity than the A315T mutation (Fig. 3K).
404 Although TDP-43 is primarily expressed in the nucleus, the aggregation of TDP-43 in the
405 cytoplasm causes toxicity. As wild-type TDP-43 may be increased in the cytoplasm if it
406 is overexpressed, it is important to realise that differences in expression levels in each

bioRxiv preprint doi: https://doi.org/10.1101/2021.10.25.465674; this version posted October 26, 2021. The copyright holder for this preprint (which was not certified by peer review) is the author/funder. All rights reserved. No reuse allowed without permission.

407 experimental system may contribute to differences in the respective results. TDP-43 may
408 also have different toxic effects on different neuronal cell types.

409 In Huntington's disease, CAG repeat expansion of *HTT* produces abnormal
410 RNA and protein, leading to neuronal dysfunction and eventual cell death. The normal
411 allele of *HTT* contains fewer than 26 CAG repeats, whereas 36 repeats or more are
412 associated with Huntington's disease [81]. A study using a mouse model of HD and
413 human patients indicated that the degeneration of the callosal axon was seen before
414 symptoms were observed, suggesting that the mutant HTT caused dying-back
415 neurodegeneration [82]. Furthermore, CAG repeat number-dependent cytotoxicity has
416 been reported in *Drosophila* [83]. In this study, as in previous reports, HTT^{Q128} showed
417 axonal toxicity but HTT^{Q0} did not (Fig. 3K).

418 Axonal degeneration is observed not only in NDs but also in Wallerian
419 degeneration (WD), which is the axotomy-induced distal degeneration of an axon,
420 causing a decline in neuronal function. The mechanisms of axonal degeneration in NDs
421 and WD are partly overlapping but not identical. Wlds is a fusion protein that slows WD;
422 it confers a protective effect from degeneration in animal models of progressive motor
423 neuropathy and PD, but does not ameliorate in ALS model [84–86]. These findings
424 suggest that each pathological protein causes axonal degeneration by a different
425 mechanism, but the detailed molecular mechanisms are still poorly understood. However,
426 by using our method, it is anticipated that research focusing on axon degeneration will be
427 facilitated, thereby enabling the elucidation of the pathological mechanism of axonal
428 degeneration by the causative genes of ND and WD. In turn, a better understanding of the
429 underlying molecular mechanisms of axonal degeneration is promising for developing
430 therapies that inhibit or delay the onset of ageing, NDs and WD.

bioRxiv preprint doi: https://doi.org/10.1101/2021.10.25.465674; this version posted October 26, 2021. The copyright holder for this preprint (which was not certified by peer review) is the author/funder. All rights reserved. No reuse allowed without permission.

By using deep learning, it was possible to automatically create a mask that extracts axon terminals from a confocal z-stack image. The image processing capabilities afforded by machine learning are powerful, and recently, many quantitative and segmentation methods using machine learning have been published [87–90]. MeDUsA is a Python-based method specifically designed to count axons; however, it only quantifies the presence of axons and does not capture pre-degenerative signs such as swelling or fragmentation of axon terminals. Such changes are currently more precisely captured only with a manual method [34]. An important future step will be to extend MeDUsA to perform a more comprehensive quantitative analysis of morphological and cell biological properties, such as the size and shape of axonal termini, the number or organisation of pre-synapses, of mitochondria or other organelles in axonal terminals, to enable more detailed studies of pathological mechanisms of ND.

Conclusions:

In this study, we developed MeDUsA for automatically quantifying the number of axons in retinal R7 neurons in *Drosophila* with high reliability and robustness. It combines pre-trained deep-learning models with a Python-based quantification system. Using our easy-to-use software, we demonstrated the causative proteins of NDs actually caused the axonal degeneration. We also confirmed that the severity of REP and axonal number were not significantly correlated. MeDUsA is a valuable tool for the unbiased and rapid quantification of axonal degeneration in genetic or pharmacological modifier screening using *Drosophila* as a model.

Materials and Methods:

bioRxiv preprint doi: https://doi.org/10.1101/2021.10.25.465674; this version posted October 26, 2021. The copyright holder for this preprint (which was not certified by peer review) is the author/funder. All rights reserved. No reuse allowed without permission.

455 ***Fly Strains***

456 Flies were maintained at 25°C on standard fly food. Female flies were used in all
457 experiments except for those shown in Figure 1 to adjust the number of retinal axons.
458 *40D-UAS* (VDRC ID 60101) was obtained from the Vienna *Drosophila* Resource Center
459 (VDRC) in Vienna, Austria. *GMR-Gal4 (III)* (#8121), *Rh6-Gal4* (#7459), *Brp-FSF-GFP*
460 (#55753), *UAS-myr-RFP* (#7119), *UAS-SNCA* (#8146), *UAS-SNCA*^{A53T} (#8148), *UAS-*
461 *Tau*^{S2A} (#51364), *tub-Gal80*^{TS} (#7017 and #7019), *UAS-marf RNAi* (#55189), *UAS-opa1*
462 *RNAi* (#32358), *GMR-w-RNAi* (#32067), *lexAop-syb-spGFP1-10*, *UAS-CD4-spGFP11*
463 (#64315) and 99 strains for RNAi screening were obtained from the Bloomington
464 *Drosophila* Stock Center (BDSC, Bloomington, IN, USA). Details are provided in Sup.
465 Table 1. *GMR-Gal4(II)* [37,38] was used for the expression of transgenes in the
466 photoreceptors. *Rh4-LexA* was generated previously [91]. *ortC2b-Gal4* was gifted by Dr.
467 Chi-Hon Lee [92], and *Sens-flippase* [93] was kindly provided by Dr. S. L. Zipursky.
468 *UAS-Tau* [5] and *UAS-Tau*^{R406W} [5] were gifted by Dr. M. B. Feany. *UAS-HTT*^{Q0} [94]and
469 *UAS-HTT*^{Q128} [94] were graciously given by the Dr. J. T. Littleton. *UAS-TDP-43(strong)*,
470 *UAS-TDP-43*^{A315T}, and *UAS-TDP43*^{G298S} were described previously [39,95].
471
472 ***Immunohistochemistry and imaging***
473 Immunohistochemistry and sample preparation were performed as described previously
474 [34,40]. The following antibodies were used: mouse anti-Chaoptin (24B10, 1:25;
475 Developmental Studies Hybridoma Bank, Iowa City, IA, USA), anti-mouse Alexa Fluor
476 488 (1:400; Thermo Fisher Scientific) and anti-mouse Alexa Fluor 568 (1:400; Thermo
477 Fisher Scientific). The insect pins were used because they are 0.1 mm in diameter and fit
478 the thickness of a fly brain. A coverslip was added and slides were mounted using

bioRxiv preprint doi: https://doi.org/10.1101/2021.10.25.465674; this version posted October 26, 2021. The copyright holder for this preprint (which was not certified by peer review) is the author/funder. All rights reserved. No reuse allowed without permission.

Vectashield mounting medium (Vector Laboratories). Images were captured using a FV3000 confocal microscope (Olympus, Tokyo, Japan). We then obtained brain images using a confocal microscope set to a 60× immersion objective (1.4 numerical aperture) and a 1× digital zoom. During the scan, we set the step size to 1 μm and generated 60–90 optical sections of the second optic ganglion medulla, including all R7 axon terminals. They are for the images shown in Figure 2, 3 and 6. In Figure 1, samples were scanned using an A1 confocal microscope (Nikon, Tokyo, Japan). Images were processed using either IMARIS 9.6.0 (Bitplane) or Fiji software, which is an open-source image analysis software [96].

Eye imaging using bright-field microscopy and quantification of morphological eye defects

For light microscopy imaging of adult eyes, 1- to 3-day-old flies, which were reared at 29°C for the expression of αSyn, Tau and HTT and at 25°C for the expression of TDP-43, were immobilised by freezing at −20°C, and separated fly heads were mounted on labelling tape (Shamrock Labels, IL, USA). The flies were then imaged using an OM-D E-M5 digital camera (Olympus) and SZX16 microscope with 6.3× magnification (Olympus). About 20 photographs were taken with the focus shifted slightly from the centre of the eye to the edges. Each slice was depth-synthesised using Photoshop CC 2017 (Adobe). The edges of the eyes were then trimmed and processed using Flynotyper 1.0 to quantitatively assess morphological defects in *Drosophila* eye [24].

Combined rough eye and axonal degeneration phenotype screening

bioRxiv preprint doi: https://doi.org/10.1101/2021.10.25.465674; this version posted October 26, 2021. The copyright holder for this preprint (which was not certified by peer review) is the author/funder. All rights reserved. No reuse allowed without permission.

First, candidate genes for screening were selected as the phenotype in the QuickSearch of FlyBase (https://flybase.org/) and searched for 'synapse' in the 'Tissue/cell affected' category. The 401 genes hit using this method were further narrowed down using settings of 'Higher' and 'Moderately High' with 'Adult Head' in the modENCODE Expression Data of FlyBase, and 99 genes available for RNAi lines at the BDSC were selected as candidate genes.

For the initial screening, we searched to identify a factor that suppressed REP to serve as an indicator of neurodegeneration. In this study, we used a transgene of TDP-43^{G298S} expressed by the eye-specific *GMR-Gal4* driver to induce REP. We then evaluated each RNAi line of the candidate genes, and the genes in which REP was suppressed were selected. We then imaged the compound eyes of *Drosophila* using an EOS Kiss X4 digital camera (Canon, Tokyo, Japan) and MZ FLIII fluorescence stereo microscope (Leica, Wetzlar, Germany).

Next, as the second screening, R8 axons were visualised to further narrow the candidate factors based on the ability to recover from axonal degeneration. To achieve this, myrRFP was expressed using the *Rh6-Gal4* driver. The genotype was *Sens-flippase/+; Rh6-Gal4/UAS-TDP-43^{G298S}; Brp-FSF-GFP, UAS-myr-RFP/UAS-RNAi*. Knockdown was performed on 15 candidate genes that suppressed the REP, and the axons were observed using an A1 confocal microscope (Nikon).

Training set generation

To quantify both normal and degenerated axons with sufficient accuracy, we used samples with phenotypes of axonal degeneration induced by either light stimulation or mitochondrial dysfunction for machine learning.

bioRxiv preprint doi: https://doi.org/10.1101/2021.10.25.465674; this version posted October 26, 2021. The copyright holder for this preprint (which was not certified by peer review) is the author/funder. All rights reserved. No reuse allowed without permission.

526 *Drosophila* photoreceptors are inherently sensory neurons for light. We found
527 that constant light stimulation caused progressive axonal degeneration [34]. Taking
528 advantage of this phenomenon, we used samples of various time points under constant
529 light from normal states to severe axonal degeneration for machine learning. In detail,
530 experimental samples at 1 (n = 16), 3 (n = 16), 5 (n = 20), 7 (n = 16), 9 (n = 14), 11 (n =
531 14) and 13 days (n = 13) under constant light were used. Samples (n = 10 and n = 19)
532 were used on day 1 and day 13 in a 12-h light/dark cycle as controls, respectively. The
533 genotype was *GMR-w-RNAi/w-; lexAop-syb-spGFP1-10, UAS-CD4-spGFP11/ Rh4-*
534 *LexA; ortC2b-Gal4/+*.

535 For machine learning, we also induced photoreceptor axonal degeneration by
536 knocking down Marf or Opa1, both of which are required for mitochondrial fusion. The
537 genotypes were *GMR-Gal4/40D-UAS; tub-Gal80^{ts}/+* (n = 6), *GMR-Gal4/UAS-marf*
538 *RNAi; tub-Gal80^{ts}/+* (n = 9) and *GMR-Gal4/tub-Gal80^{ts}; UAS-opa1 RNAi/+* (n = 20).
539 The flies were reared in a permissive temperature (20°C), and after eclosion, knockdown
540 was induced by rearing the flies in a restrictive temperature (29°C) and were dissected 4
541 weeks later. Samples reared under control conditions at 20°C for 4 weeks after eclosion
542 were also used for machine learning. The genotypes were *GMR-Gal4/40D-UAS; tub-*
543 *Gal80^{ts}/+* (n = 14), *GMR-Gal4/UAS-marf RNAi; tub-Gal80^{ts}/+* (n = 20), and *GMR-*
544 *Gal4/tub-Gal80^{ts}; UAS-opa1 RNAi/+* (n = 10).

545 All samples were scanned using a confocal microscope. We then manually
546 created a mask covering the axonal terminal and used the scanning data and the mask as
547 a training set.

548

549 ***Surface mask prediction and axon terminal detection***

bioRxiv preprint doi: https://doi.org/10.1101/2021.10.25.465674; this version posted October 26, 2021. The copyright holder for this preprint (which was not certified by peer review) is the author/funder. All rights reserved. No reuse allowed without permission.

A variant of 2D-U-Net was used for surface mask prediction. The original images were N × 512 × 512 in size for each sample, and for each z-slice, the image before and after it (z − 1, z and z + 1) were combined to form the N × 512 × 512 × 3 size. As the terminal slice does not have z − 1 or z + 1, a blank image was used instead. For training, we used mask images of size N × 512 × 512 × 3, and for inference, we obtained mask prediction images of size N × 512 × 512 by discarding the channels corresponding to each z − 1 and z + 1 from the N × 512 × 512 × 3 output and retaining only z. As post-processing, opening and closing operations were used to exclude small blobs and to fill in holes. Then, from the original image, only the area corresponding to the obtained surface mask image was extracted. To detect the axon terminal, the background image was first created by morphological reconstruction and then filtered regional maxima by subtracting it from the original image to remove the background. Next, the image was binarised by adaptive thresholding, and 3D watershed was performed using the peak obtained by calculating the Euclidean distance as a seed. Finally, blobs below 20 voxels were excluded. These processes were calculated using Python (v3.6.7), NumPy (v1.17.3), TensorFlow (v1.13.2), scikit-image (v0.16.2), SciPy (v1.3.2) and OpenCV (v4.2.0).

Experimental design and statistical analyses

Experimental analyses were performed using Prism 8 (GraphPad Software, San Diego, CA, USA). All quantifications were performed by experimenters who were blind to the genotype. Data were analysed using multiple comparison ANOVA with Tukey–Kramer post hoc tests or unpaired t-test with Mann–Whitney test, as noted in the Results section. The null hypothesis was rejected at a 0.05 level of significance.

bioRxiv preprint doi: https://doi.org/10.1101/2021.10.25.465674; this version posted October 26, 2021. The copyright holder for this preprint (which was not certified by peer review) is the author/funder. All rights reserved. No reuse allowed without permission.

List of Abbreviations:

MeDUsA : a method for quantification of degeneration using fly axons

ND: Neurodegenerative disease

REP: rough eye phenotype

SCA3: Spinocerebellar ataxia type 3

PD: Parkinson's disease

ALS: amyotrophic lateral sclerosis

CNN: convolutional neural network

RNAi: RNA interference

SCA31: spinocerebellar ataxia type 31

FTLD: frontotemporal lobar degeneration

WD: Wallerian degeneration

Declarations

Ethics approval and consent to participate

Not applicable

Consent for publication

Not applicable

Availability of data and materials

The software documentation for MeDUsA can be found at

https://github.com/SugieLab/MeDUsA.

bioRxiv preprint doi: https://doi.org/10.1101/2021.10.25.465674; this version posted October 26, 2021. The copyright holder for this preprint (which was not certified by peer review) is the author/funder. All rights reserved. No reuse allowed without permission.

The datasets used and/or analyzed during the current study are available from the corresponding authors on reasonable request.

Competing interests

The authors declare that we have no competing interests.

Funding

This work was supported in part by grants from the Ministry of Education, Culture, Sports, Science and Technology of Japan (#18K14835, #18J00367 and #21K15619 to YNI, #21K06184 to SHS, #17H05699 to YNA, #16H06457 and #21H02483 to TS, #17H04983, #19K22592 and #21H02837 to AS), grants for Strategic Research Program for Brain Sciences from Japan Agency for Medical Research and Development, Japan (#JP20dm0107061 to YNA), Takeda Science Foundation Takeda Visionary Research Grant to T.S., and Takeda science foundation life science research grant to AS. DZNE core funding to G.T.

Authors' contributions

YNI and AS designed and organized the study.

YNI and AS performed immunohistochemistry, and eye imaging.

YNI, AS and KD performed data analysis.

HK established the software.

JO, SHS, and TS designed the screen experiment and JO performed the experiment and data analysis.

YNA generated transgenic flies.

bioRxiv preprint doi: https://doi.org/10.1101/2021.10.25.465674; this version posted October 26, 2021. The copyright holder for this preprint (which was not certified by peer review) is the author/funder. All rights reserved. No reuse allowed without permission.

YNI, HK, KD, GT and AS wrote the manuscript

All authors read and approved the final manuscript.

Acknowledgements

We would like to acknowledge that Dr. Zipursky, Dr. Feany, Dr. Lee and Dr. Littleton have provided us with transgenic fly strains. We would like to thank Ms. Nozaki for helping us to quantify REP.

Figure Legends:

Figure 1. Rough eye and axonal degeneration phenotypes for evaluating neurodegeneration.

(A) Dorsal schematic of the visual system in *Drosophila*. The axons of photoreceptors R7 and R8 project from the retina through the lamina to the medulla. (B) The process of exploring factors that mitigate TDP-43 toxicity using a combination of rough eye and axonal degeneration phenotypic observations. (C) Candidate genes that suppress the rough eye phenotype (REP) and their involvement in axonal toxicity. In knockdown screening, six genes suppressed REP and eight genes mildly suppressed it. However, the degree of REP and severity of R axon degeneration were not consistent. Yellow arrows indicate fragmented axons. Scale bar = 20 μm. (D) Quantification of the ratio of axonal degeneration. ***$p < 0.001$. Chi-square test was performed between the control and each knockdown.

Figure 2. Sample Preparation and Processing flow of MeDUsA.

bioRxiv preprint doi: https://doi.org/10.1101/2021.10.25.465674; this version posted October 26, 2021. The copyright holder for this preprint (which was not certified by peer review) is the author/funder. All rights reserved. No reuse allowed without permission.

(A) Schematic of the visual system in *Drosophila*. (B) All R7 and R8 axon terminals projecting to the medulla. R axons were stained with anti-Chaoptin, which is a photoreceptor-specific antibody (green). Scale bar = 20 μm. (C) Process flow of generating a surface mask. First, for each slice of the z-stack image, three slices ($z - 1$, z and $z + 1$) are merged by adding the previous and next slice to create an RGB image. The RGB image is inputted into the training model to generate the RGB mask. Finally, only the channel corresponding to the central slice is extracted to obtain the final mask. (D) Process for axon terminal detection. Using the obtained surface mask stack and original image stack, the surface mask region is extracted from the original image for each slice, and only the signal at the axon end is extracted. Axon terminals are then detected and quantified from the obtained 3D volume.

Figure 3. Toxicity evaluation of representative ND causative factors using MeDUsA.

(A–J) The R axon terminals stained with anti-Chaoptin and extracted using MeDUsA. (A) Control and photoreceptor expression of (B) αSyn^{WT}, (C) αSyn^{A53T}, (D) Tau^{WT}, (E) Tau^{R406W}, (F) Tau^{S2A}, (G) $TDP\text{-}43^{WT}$, (H) $TDP\text{-}43^{A315T}$, (I) HTT^{Q0} and (J) HTT^{Q128}. Scale bar = 20 μm. (K) The number of axons expressing each pathogenic factor was predicted. $^{****}p < 0.0001$, $^{***}p < 0.001$ and ns ($p > 0.05$). Data were analysed using multiple comparison ANOVA with Tukey–Kramer *post hoc* tests. Error bars show the standard error of the mean.

Figure 4. Comparison between manual quantification and the MeDUsA system.

(A) The axonal numbers quantified by manual measurements using the same dataset shown in Figure 3K. $^{****}p < 0.00001$, $^{***}p < 0.001$, $^{**}p < 0.01$, $^{*}p < 0.05$ and ns ($p >$

bioRxiv preprint doi: https://doi.org/10.1101/2021.10.25.465674; this version posted October 26, 2021. The copyright holder for this preprint (which was not certified by peer review) is the author/funder. All rights reserved. No reuse allowed without permission.

668 0.05). Data were analysed using multiple comparison ANOVA with Tukey–Kramer post
669 hoc tests. Error bars show the standard error of the mean. (B) The ratio of the axonal
670 number predicted by MeDUsA to those measured manually for each genotype. (C) The
671 correlation between the individual values measured manually and the individual values
672 predicted by MeDUsA. (D) The correlation between the average of each genotype
673 measured manually versus those predicted by MeDUsA. R^2, coefficient of determination.
674
675 **Figure 5. Ectopic expression of causative genes of NDs in fly eye causing REP, but**
676 **inconsistent with axonal degeneration.**
677 (A–J) Representative bright-field microscope images of (A) control or fly eyes
678 overexpressing (B) $SNCA^{WT}$, (C) $SNCA^{A53T}$, (D) Tau^{WT}, (E) Tau^{R406W}, (F) Tau^{S2A}, (G)
679 $TDP\text{-}43^{WT}$, (H) $TDP\text{-}43^{A315T}$, (I) HTT^{Q0} and (J) HTT^{Q128} using the GMR-Gal4 driver. (K)
680 Graph representing the phenotypic score (P score) of each genotype calculated using
681 Flynotyper. ****$p < 0.0001$, **$p < 0.01$ and ns ($p > 0.05$). Data were analysed using
682 multiple comparison ANOVA with Tukey–Kramer *post hoc* tests. Error bars show the
683 standard error of the mean.
684
685 **Reference**
686

687 1. Dugger BN, Dickson DW. Pathology of Neurodegenerative Diseases. Csh Perspect
688 Biol. 2017;9:a028035.

bioRxiv preprint doi: https://doi.org/10.1101/2021.10.25.465674; this version posted October 26, 2021. The copyright holder for this preprint (which was not certified by peer review) is the author/funder. All rights reserved. No reuse allowed without permission.

689 2. Warrick JM, Paulson HL, Gray-Board GL, Bui QT, Fischbeck KH, Pittman RN, et al.
690 Expanded Polyglutamine Protein Forms Nuclear Inclusions and Causes Neural
691 Degeneration in Drosophila. Cell. 1998;93:939–49.

692 3. Jackson GR, Salecker I, Dong X, Yao X, Arnheim N, Faber PW, et al.
693 Polyglutamine-Expanded Human Huntingtin Transgenes Induce Degeneration of
694 Drosophila Photoreceptor Neurons. Neuron. 1998;21:633–42.

695 4. Feany MB, Bender WW. A Drosophila model of Parkinson's disease. Nature.
696 2000;404:394–8.

697 5. Wittmann CW, Wszolek MF, Shulman JM, Salvaterra PM, Lewis J, Hutton M, et al.
698 Tauopathy in Drosophila: neurodegeneration without neurofibrillary tangles. Science.
699 2001;293:711–4.

700 6. Chouhan AK, Guo C, Hsieh Y-C, Ye H, Senturk M, Zuo Z, et al. Uncoupling
701 neuronal death and dysfunction in Drosophila models of neurodegenerative disease.
702 Acta Neuropathologica Commun. 2016;4:62.

703 7. Elden AC, Kim H-J, Hart MP, Chen-Plotkin AS, Johnson BS, Fang X, et al. Ataxin-2
704 intermediate-length polyglutamine expansions are associated with increased risk for
705 ALS. Nature. 2010;466:1069–75.

706 8. Brand AH, Perrimon N. Targeted gene expression as a means of altering cell fates
707 and generating dominant phenotypes. Development. 1993;118:401–15.

bioRxiv preprint doi: https://doi.org/10.1101/2021.10.25.465674; this version posted October 26, 2021. The copyright holder for this preprint (which was not certified by peer review) is the author/funder. All rights reserved. No reuse allowed without permission.

9. Blard O, Feuillette S, Bou J, Chaumette B, Frébourg T, Campion D, et al. Cytoskeleton proteins are modulators of mutant tau-induced neurodegeneration in Drosophila. Hum Mol Genet. 2007;16:555–66.

10. Chen X, Li Y, Huang J, Cao D, Yang G, Liu W, et al. Study of tauopathies by comparing Drosophila and human tau in Drosophila. Cell Tissue Res. 2007;329:169–78.

11. Ambegaokar SS, Jackson GR. Functional genomic screen and network analysis reveal novel modifiers of tauopathy dissociated from tau phosphorylation. Hum Mol Genet. 2011;20:4947–77.

12. M'Angale PG, Staveley BE. The Bcl-2 homologue Buffy rescues α-synuclein-induced Parkinson disease-like phenotypes in Drosophila. Bmc Neurosci. 2016;17:24.

13. Alexopoulou Z, Lang J, Perrett RM, Elschami M, Hurry MED, Kim HT, et al. Deubiquitinase Usp8 regulates α-synuclein clearance and modifies its toxicity in Lewy body disease. Proc National Acad Sci. 2016;113:E4688–97.

14. Davies SE, Hallett PJ, Moens T, Smith G, Mangano E, Kim HT, et al. Enhanced ubiquitin-dependent degradation by Nedd4 protects against α-synuclein accumulation and toxicity in animal models of Parkinson's disease. Neurobiol Dis. 2014;64:79–87.

15. Miura E, Hasegawa T, Konno M, Suzuki M, Sugeno N, Fujikake N, et al. VPS35 dysfunction impairs lysosomal degradation of α-synuclein and exacerbates neurotoxicity in a Drosophila model of Parkinson's disease. Neurobiol Dis. 2014;71:1–13.

bioRxiv preprint doi: https://doi.org/10.1101/2021.10.25.465674; this version posted October 26, 2021. The copyright holder for this preprint (which was not certified by peer review) is the author/funder. All rights reserved. No reuse allowed without permission.

729 16. Zhan L, Hanson KA, Kim SH, Tare A, Tibbetts RS. Identification of Genetic
730 Modifiers of TDP-43 Neurotoxicity in Drosophila. Plos One. 2013;8:e57214.

731 17. Kim H-J, Raphael AR, LaDow ES, McGurk L, Weber RA, Trojanowski JQ, et al.
732 Therapeutic modulation of eIF2α phosphorylation rescues TDP-43 toxicity in
733 amyotrophic lateral sclerosis disease models. Nat Genet. 2014;46:152–60.

734 18. Calpena E, Amo VL del, Chakraborty M, Llamusí B, Artero R, Espinós C, et al. The
735 Drosophila junctophilin gene is functionally equivalent to its four mammalian
736 counterparts and is a modifier of a Huntingtin poly-Q expansion and the Notch
737 pathway. Dis Model Mech. 2017;11:dmm029082.

738 19. Kaltenbach LS, Orr H, Romero E, Becklin RR, Chettier R, Bell R, et al. Huntingtin
739 interacting proteins are genetic modifiers of neurodegeneration. PLoS Genetics.
740 2007;3:e82.

741 20. Doumanis J, Wada K, Kino Y, Moore AW, Nukina N. RNAi Screening in
742 Drosophila Cells Identifies New Modifiers of Mutant Huntingtin Aggregation. Plos
743 One. 2009;4:e7275.

744 21. Shim K-H, Kim S-H, Hur J, Kim D-H, Demirev AV, Yoon S-Y. Small-molecule
745 drug screening identifies drug Ro 31-8220 that reduces toxic phosphorylated tau in
746 Drosophila melanogaster. Neurobiol Dis. 2019;130:104519.

747 22. Lin Y, Xue J, Deng J, He H, Luo S, Chen J, et al. Neddylation activity modulates
748 the neurodegeneration associated with fragile X associated tremor/ataxia syndrome
749 (FXTAS) through regulating Sima. Neurobiol Dis. 2020;143:105013.

bioRxiv preprint doi: https://doi.org/10.1101/2021.10.25.465674; this version posted October 26, 2021. The copyright holder for this preprint (which was not certified by peer review) is the author/funder. All rights reserved. No reuse allowed without permission.

750 23. Diez-Hermano S, Valero J, Rueda C, Ganfornina MD, Sanchez D. An automated
751 image analysis method to measure regularity in biological patterns: a case study in a
752 Drosophila neurodegenerative model. Molecular neurodegeneration. 2015;10:9.

753 24. Iyer J, Wang Q, Le T, Pizzo L, Grönke S, Ambegaokar SS, et al. Quantitative
754 Assessment of Eye Phenotypes for Functional Genetic Studies Using Drosophila
755 melanogaster. G3 (Bethesda, Md). 2016;6:1427–37.

756 25. McGurk L, Berson A, Bonini NM. Drosophila as an In Vivo Model for Human
757 Neurodegenerative Disease. Genetics. 2015;201:377–402.

758 26. Bhattacharya MRC, Gerdts J, Naylor SA, Royse EX, Ebstein SY, Sasaki Y, et al. A
759 model of toxic neuropathy in Drosophila reveals a role for MORN4 in promoting
760 axonal degeneration. Journal of Neuroscience. 2012;32:5054–61.

761 27. Sreedharan J, Neukomm LJ, Brown RH, Freeman MR. Age-Dependent TDP-43-
762 Mediated Motor Neuron Degeneration Requires GSK3, hat-trick, and xmas-2. Curr
763 Biol. 2015;25:2130–6.

764 28. Moen E, Bannon D, Kudo T, Graf W, Covert M, Valen DV. Deep learning for
765 cellular image analysis. Nat Methods. 2019;16:1233–46.

766 29. Ronneberger O, Fischer P, Brox T. U-Net: Convolutional Networks for Biomedical
767 Image Segmentation. Lect Notes Comput Sc. 2015;234–41.

768 30. Çiçek Ö, Abdulkadir A, Lienkamp SS, Brox T, Ronneberger O. 3D U-Net: Learning
769 Dense Volumetric Segmentation from Sparse Annotation. Medical Image Computing

bioRxiv preprint doi: https://doi.org/10.1101/2021.10.25.465674; this version posted October 26, 2021. The copyright holder for this preprint (which was not certified by peer review) is the author/funder. All rights reserved. No reuse allowed without permission.

and Computer-Assisted Intervention – MICCAI 2016, 19th International Conference, Athens, Greece, October 17-21, 2016, Proceedings, Part II. 2016. p. 424–32.

31. Falk T, Mai D, Bensch R, Çiçek Ö, Abdulkadir A, Marrakchi Y, et al. U-Net: deep learning for cell counting, detection, and morphometry. Nat Methods. 2019;16:67–70.

32. Fischer CA, Besora-Casals L, Rolland SG, Haeussler S, Singh K, Duchen M, et al. MitoSegNet: Easy-to-use Deep Learning Segmentation for Analyzing Mitochondrial Morphology. iScience. 2020;23:101601.

33. Long F. Microscopy cell nuclei segmentation with enhanced U-Net. Bmc Bioinformatics. 2020;21:8.

34. Richard M, Doubková K, Nitta Y, Kawai H, Sugie A, Tavosanis G. A quantitative model of sporadic axonal degeneration in the Drosophila visual system. bioRxiv. 2021;

35. Sang T-K, Jackson GR. Drosophila models of neurodegenerative disease. Neurorx. 2005;2:438–46.

36. Deerlin VMV, Leverenz JB, Bekris LM, Bird TD, Yuan W, Elman LB, et al. TARDBP mutations in amyotrophic lateral sclerosis with TDP-43 neuropathology: a genetic and histopathological analysis. Lancet Neurology. 2008;7:409–16.

37. Newsome TP, Asling B, Dickson BJ. Analysis of Drosophila photoreceptor axon guidance in eye-specific mosaics. Development. 2000;127:851–60.

bioRxiv preprint doi: https://doi.org/10.1101/2021.10.25.465674; this version posted October 26, 2021. The copyright holder for this preprint (which was not certified by peer review) is the author/funder. All rights reserved. No reuse allowed without permission.

788 38. Newsome TP, Schmidt S, Dietzl G, Keleman K, Asling B, Debant A, et al. Trio
789 combines with dock to regulate Pak activity during photoreceptor axon pathfinding in
790 Drosophila. Cell. 2000;101:283–94.

791 39. Ishiguro T, Sato N, Ueyama M, Fujikake N, Sellier C, Kanegami A, et al.
792 Regulatory Role of RNA Chaperone TDP-43 for RNA Misfolding and Repeat-
793 Associated Translation in SCA31. Neuron. 2017;94:108-124.e7.

794 40. Sugie A, Möhl C, Hakeda-Suzuki S, Matsui H, Suzuki T, Tavosanis G. Analyzing
795 Synaptic Modulation of Drosophila melanogaster Photoreceptors after Exposure to
796 Prolonged Light. J Vis Exp. 2017;

797 41. Spillantini MG, Schmidt ML, Lee VM-Y, Trojanowski JQ, Jakes R, Goedert M. α-
798 Synuclein in Lewy bodies. Nature. 1997;388:839–40.

799 42. Polymeropoulos MH, Lavedan C, Leroy E, Ide SE, Dehejia A, Dutra A, et al.
800 Mutation in the α-Synuclein Gene Identified in Families with Parkinson9s Disease.
801 Science. 1997;276:2045–7.

802 43. Hutton M, Lendon CL, Rizzu P, Baker M, Froelich S, Houlden H, et al. Association
803 of missense and 5′-splice-site mutations in tau with the inherited dementia FTDP-17.
804 Nature. 1998;393:702–5.

805 44. Gitcho MA, Baloh RH, Chakraverty S, Mayo K, Norton JB, Levitch D, et al. TDP-
806 43 A315T mutation in familial motor neuron disease. Ann Neurol. 2008;63:535–8.

bioRxiv preprint doi: https://doi.org/10.1101/2021.10.25.465674; this version posted October 26, 2021. The copyright holder for this preprint (which was not certified by peer review) is the author/funder. All rights reserved. No reuse allowed without permission.

807 45. Chen X, Peterson J, Nachman RJ, Ganetzky B. Drosulfakinin activates CCKLR-
808 17D1 and promotes larval locomotion and escape response in Drosophila. Fly.
809 2012;6:290–7.

810 46. Williams MJ, Goergen P, Rajendran J, Zheleznyakova G, Hägglund MG, Perland E,
811 et al. Obesity-Linked Homologues TfAP-2 and Twz Establish Meal Frequency in
812 Drosophila melanogaster. Plos Genet. 2014;10:e1004499.

813 47. Agrawal P, Kao D, Chung P, Looger LL. The neuropeptide Drosulfakinin regulates
814 social isolation-induced aggression in Drosophila. J Exp Biol. 2020;223:jeb207407.

815 48. Wu F, Deng B, Xiao N, Wang T, Li Y, Wang R, et al. A neuropeptide regulates
816 fighting behavior in Drosophila melanogaster. Elife. 2020;9:e54229.

817 49. Chen X, Ganetzky B. A neuropeptide signaling pathway regulates synaptic growth
818 in Drosophila. J Cell Biol. 2012;196:529–43.

819 50. Fogarty MJ, Klenowski PM, Lee JD, Drieberg-Thompson JR, Bartlett SE, Ngo ST,
820 et al. Cortical synaptic and dendritic spine abnormalities in a presymptomatic TDP-43
821 model of amyotrophic lateral sclerosis. Sci Rep-uk. 2016;6:37968.

822 51. Jiang T, Handley E, Brizuela M, Dawkins E, Lewis KEA, Clark RM, et al.
823 Amyotrophic lateral sclerosis mutant TDP-43 may cause synaptic dysfunction through
824 altered dendritic spine function. Dis Model Mech. 2019;12:dmm038109.

825 52. Breen TR, Lucchesi JC. Analysis of the dosage compensation of a specific transcript
826 in Drosophila melanogaster. Genetics. 1986;112:483–91.

bioRxiv preprint doi: https://doi.org/10.1101/2021.10.25.465674; this version posted October 26, 2021. The copyright holder for this preprint (which was not certified by peer review) is the author/funder. All rights reserved. No reuse allowed without permission.

827 53. Freibaum BD, Chitta RK, High AA, Taylor JP. Global Analysis of TDP-43
828 Interacting Proteins Reveals Strong Association with RNA Splicing and Translation
829 Machinery. J Proteome Res. 2010;9:1104–20.

830 54. Kim SH, Shanware NP, Bowler MJ, Tibbetts RS. Amyotrophic Lateral Sclerosis-
831 associated Proteins TDP-43 and FUS/TLS Function in a Common Biochemical
832 Complex to Co-regulate HDAC6 mRNA*. J Biol Chem. 2010;285:34097–105.

833 55. Ling S-C, Albuquerque CP, Han JS, Lagier-Tourenne C, Tokunaga S, Zhou H, et al.
834 ALS-associated mutations in TDP-43 increase its stability and promote TDP-43
835 complexes with FUS/TLS. Proc National Acad Sci. 2010;107:13318–23.

836 56. Wang J-W, Brent JR, Tomlinson A, Shneider NA, McCabe BD. The ALS-
837 associated proteins FUS and TDP-43 function together to affect Drosophila locomotion
838 and life span. J Clin Invest. 2011;121:4118–26.

839 57. Kabashi E, Bercier V, Lissouba A, Liao M, Brustein E, Rouleau GA, et al. FUS and
840 TARDBP but Not SOD1 Interact in Genetic Models of Amyotrophic Lateral Sclerosis.
841 Plos Genet. 2011;7:e1002214.

842 58. Lee S, Wang J-W, Yu W, Lu B. Phospho-dependent ubiquitination and degradation
843 of PAR-1 regulates synaptic morphology and tau-mediated Aβ toxicity in Drosophila.
844 Nature Communications. 2012;3:1312–12.

845 59. Burré J, Sharma M, Südhof TC. Cell Biology and Pathophysiology of α-Synuclein.
846 Csh Perspect Med. 2018;8:a024091.

bioRxiv preprint doi: https://doi.org/10.1101/2021.10.25.465674; this version posted October 26, 2021. The copyright holder for this preprint (which was not certified by peer review) is the author/funder. All rights reserved. No reuse allowed without permission.

847 60. Orimo S, Uchihara T, Nakamura A, Mori F, Kakita A, Wakabayashi K, et al.
848 Axonal α-synuclein aggregates herald centripetal degeneration of cardiac sympathetic
849 nerve in Parkinson's disease. Brain. 2008;131:642–50.

850 61. Volpicelli-Daley LA, Luk KC, Patel TP, Tanik SA, Riddle DM, Stieber A, et al.
851 Exogenous α-Synuclein Fibrils Induce Lewy Body Pathology Leading to Synaptic
852 Dysfunction and Neuron Death. Neuron. 2011;72:57–71.

853 62. Lashuel HA, Overk CR, Oueslati A, Masliah E. The many faces of α-synuclein:
854 from structure and toxicity to therapeutic target. Nature Publishing Group. 2013;14:38–
855 48.

856 63. Kouroupi G, Taoufik E, Vlachos IS, Tsioras K, Antoniou N, Papastefanaki F, et al.
857 Defective synaptic connectivity and axonal neuropathology in a human iPSC-based
858 model of familial Parkinson's disease. Proc National Acad Sci. 2017;114:E3679–88.

859 64. Bengoa-Vergniory N, Roberts RF, Wade-Martins R, Alegre-Abarrategui J. Alpha-
860 synuclein oligomers: a new hope. Acta Neuropathologica. 2017;134:819–38.

861 65. Kolarova M, García-Sierra F, Bartos A, Ricny J, Ripova D. Structure and Pathology
862 of Tau Protein in Alzheimer Disease. Int J Alzheimer's Dis. 2012;2012:731526.

863 66. Dayanandan R, Slegtenhorst MV, Mack TGA, Ko L, Yen S-H, Leroy K, et al.
864 Mutations in tau reduce its microtubule binding properties in intact cells and affect its
865 phosphorylation. Febs Lett. 1999;446:228–32.

bioRxiv preprint doi: https://doi.org/10.1101/2021.10.25.465674; this version posted October 26, 2021. The copyright holder for this preprint (which was not certified by peer review) is the author/funder. All rights reserved. No reuse allowed without permission.

866 67. Miyasaka T, Morishima-Kawashima M, Ravid R, Heutink P, Swieten JC van,
867 Nagashima K, et al. Molecular Analysis of Mutant and Wild-Type Tau Deposited in the
868 Brain Affected by the FTDP-17 R406W Mutation. Am J Pathology. 2001;158:373–9.

869 68. Ikeda M, Kawarai T, Kawarabayashi T, Matsubara E, Murakami T, Sasaki A, et al.
870 Accumulation of Filamentous Tau in the Cerebral Cortex of Human Tau R406W
871 Transgenic Mice. Am J Pathology. 2005;166:521–31.

872 69. Nakamura M, Shiozawa S, Tsuboi D, Amano M, Watanabe H, Maeda S, et al.
873 Pathological Progression Induced by the Frontotemporal Dementia-Associated R406W
874 Tau Mutation in Patient-Derived iPSCs. Stem Cell Rep. 2019;13:684–99.

875 70. Jackson GR, Wiedau-Pazos M, Sang T-K, Wagle N, Brown CA, Massachi S, et al.
876 Human Wild-Type Tau Interacts with wingless Pathway Components and Produces
877 Neurofibrillary Pathology in Drosophila. Neuron. 2002;34:509–19.

878 71. Povellato G, Tuxworth RI, Hanger DP, Tear G. Modification of the Drosophila
879 model of in vivo Tau toxicity reveals protective phosphorylation by GSK3β. Biol Open.
880 2013;3:1–11.

881 72. Neumann M, Sampathu DM, Kwong LK, Truax AC, Micsenyi MC, Chou TT, et al.
882 Ubiquitinated TDP-43 in Frontotemporal Lobar Degeneration and Amyotrophic Lateral
883 Sclerosis. Science. 2006;314:130–3.

884 73. Prasad A, Bharathi V, Sivalingam V, Girdhar A, Patel BK. Molecular Mechanisms
885 of TDP-43 Misfolding and Pathology in Amyotrophic Lateral Sclerosis. Front Mol
886 Neurosci. 2019;12:25.

bioRxiv preprint doi: https://doi.org/10.1101/2021.10.25.465674; this version posted October 26, 2021. The copyright holder for this preprint (which was not certified by peer review) is the author/funder. All rights reserved. No reuse allowed without permission.

887 74. Kabashi E, Lin L, Tradewell ML, Dion PA, Bercier V, Bourgouin P, et al. Gain and
888 loss of function of ALS-related mutations of TARDBP (TDP-43) cause motor deficits
889 in vivo. Hum Mol Genet. 2010;19:671–83.

890 75. Xu Y-F, Gendron TF, Zhang Y-J, Lin W-L, D'Alton S, Sheng H, et al. Wild-Type
891 Human TDP-43 Expression Causes TDP-43 Phosphorylation, Mitochondrial
892 Aggregation, Motor Deficits, and Early Mortality in Transgenic Mice. J Neurosci.
893 2010;30:10851–9.

894 76. Ash PEA, Zhang Y-J, Roberts CM, Saldi T, Hutter H, Buratti E, et al. Neurotoxic
895 effects of TDP-43 overexpression in C. elegans. Hum Mol Genet. 2010;19:3206–18.

896 77. Diaper DC, Adachi Y, Sutcliffe B, Humphrey DM, Elliott CJH, Stepto A, et al. Loss
897 and gain of Drosophila TDP-43 impair synaptic efficacy and motor control leading to
898 age-related neurodegeneration by loss-of-function phenotypes. Hum Mol Genet.
899 2013;22:1539–57.

900 78. Li Y, Ray P, Rao EJ, Shi C, Guo W, Chen X, et al. A Drosophila model for TDP-43
901 proteinopathy. Proc National Acad Sci. 2010;107:3169–74.

902 79. Guo W, Chen Y, Zhou X, Kar A, Ray P, Chen X, et al. An ALS-associated mutation
903 affecting TDP-43 enhances protein aggregation, fibril formation and neurotoxicity. Nat
904 Struct Mol Biol. 2011;18:822–30.

905 80. Estes PS, Boehringer A, Zwick R, Tang JE, Grigsby B, Zarnescu DC. Wild-type
906 and A315T mutant TDP-43 exert differential neurotoxicity in a Drosophila model of
907 ALS. Hum Mol Genet. 2011;20:2308–21.

bioRxiv preprint doi: https://doi.org/10.1101/2021.10.25.465674; this version posted October 26, 2021. The copyright holder for this preprint (which was not certified by peer review) is the author/funder. All rights reserved. No reuse allowed without permission.

908 81. Roos RA. Huntington's disease: a clinical review. Orphanet J Rare Dis. 2010;5:40.

909 82. Gatto RG, Chu Y, Ye AQ, Price SD, Tavassoli E, Buenaventura A, et al. Analysis
910 of YFP(J16)-R6/2 reporter mice and postmortem brains reveals early pathology and
911 increased vulnerability of callosal axons in Huntington's disease. Hum Mol Genet.
912 2015;24:5285–98.

913 83. Zhang S, Binari R, Zhou R, Perrimon N. A Genomewide RNA Interference Screen
914 for Modifiers of Aggregates Formation by Mutant Huntingtin in Drosophila. Genetics.
915 2010;184:1165–79.

916 84. Ferri A, Sanes JR, Coleman MP, Cunningham JM, Kato AC. Inhibiting Axon
917 Degeneration and Synapse Loss Attenuates Apoptosis and Disease Progression in a
918 Mouse Model of Motoneuron Disease. Curr Biol. 2003;13:669–73.

919 85. Sajadi A, Schneider BL, Aebischer P. Wlds-Mediated Protection of Dopaminergic
920 Fibers in an Animal Model of Parkinson Disease. Curr Biol. 2004;14:326–30.

921 86. Velde CV, Garcia ML, Yin X, Trapp BD, Cleveland DW. The neuroprotective
922 factor Wlds does not attenuate mutant SOD1-mediated motor neuron disease. Neuromol
923 Med. 2004;5:193–203.

924 87. Haberl MG, Churas C, Tindall L, Boassa D, Phan S, Bushong EA, et al.
925 CDeep3M—Plug-and-Play cloud-based deep learning for image segmentation. Nat
926 Methods. 2018;15:677–80.

bioRxiv preprint doi: https://doi.org/10.1101/2021.10.25.465674; this version posted October 26, 2021. The copyright holder for this preprint (which was not certified by peer review) is the author/funder. All rights reserved. No reuse allowed without permission.

927 88. Diez-Hermano S, Ganfornina MD, Vegas-Lozano E, Sanchez D. Machine Learning
928 Representation of Loss of Eye Regularity in a Drosophila Neurodegenerative Model.
929 Front Neurosci-switz. 2020;14:516.

930 89. Kayasandik CB, Ru W, Labate D. A multistep deep learning framework for the
931 automated detection and segmentation of astrocytes in fluorescent images of brain
932 tissue. Sci Rep-uk. 2020;10:5137.

933 90. Fogo GM, Anzell AR, Maheras KJ, Raghunayakula S, Wider JM, Emaus KJ, et al.
934 Machine learning-based classification of mitochondrial morphology in primary neurons
935 and brain. Sci Rep-uk. 2021;11:5133.

936 91. Berger-Müller S, Sugie A, Takahashi F, Tavosanis G, Hakeda-Suzuki S, Suzuki T.
937 Assessing the Role of Cell-Surface Molecules in Central Synaptogenesis in the
938 Drosophila Visual System. Plos One. 2013;8:e83732.

939 92. Gao S, Takemura S, Ting C-Y, Huang S, Lu Z, Luan H, et al. The Neural Substrate
940 of Spectral Preference in Drosophila. Neuron. 2008;60:328–42.

941 93. Chen Y, Akin O, Nern A, Tsui CYK, Pecot MY, Zipursky SL. Cell-type-Specific
942 Labeling of Synapses In Vivo through Synaptic Tagging with Recombination. Neuron.
943 2014;81:280–93.

944 94. Lee W-CM, Yoshihara M, Littleton JT. Cytoplasmic aggregates trap polyglutamine-
945 containing proteins and block axonal transport in a Drosophila model of Huntington's
946 disease. P Natl Acad Sci Usa. 2004;101:3224–9.

bioRxiv preprint doi: https://doi.org/10.1101/2021.10.25.465674; this version posted October 26, 2021. The copyright holder for this preprint (which was not certified by peer review) is the author/funder. All rights reserved. No reuse allowed without permission.

947 95. Saitoh Y, Fujikake N, Okamoto Y, Popiel HA, Hatanaka Y, Ueyama M, et al. p62
948 Plays a Protective Role in the Autophagic Degradation of Polyglutamine Protein
949 Oligomers in Polyglutamine Disease Model Flies*. J Biol Chem. 2015;290:1442–53.

950 96. Schindelin J, Arganda-Carreras I, Frise E, Kaynig V, Longair M, Pietzsch T, et al.
951 Fiji: an open-source platform for biological-image analysis. Nature Methods.
952 2012;9:676–82.

953

bioRxiv preprint doi: https://doi.org/10.1101/2021.10.25.465674; this version posted October 26, 2021. The copyright holder for this preprint (which was not certified by peer review) is the author/funder. All rights reserved. No reuse allowed without permission.

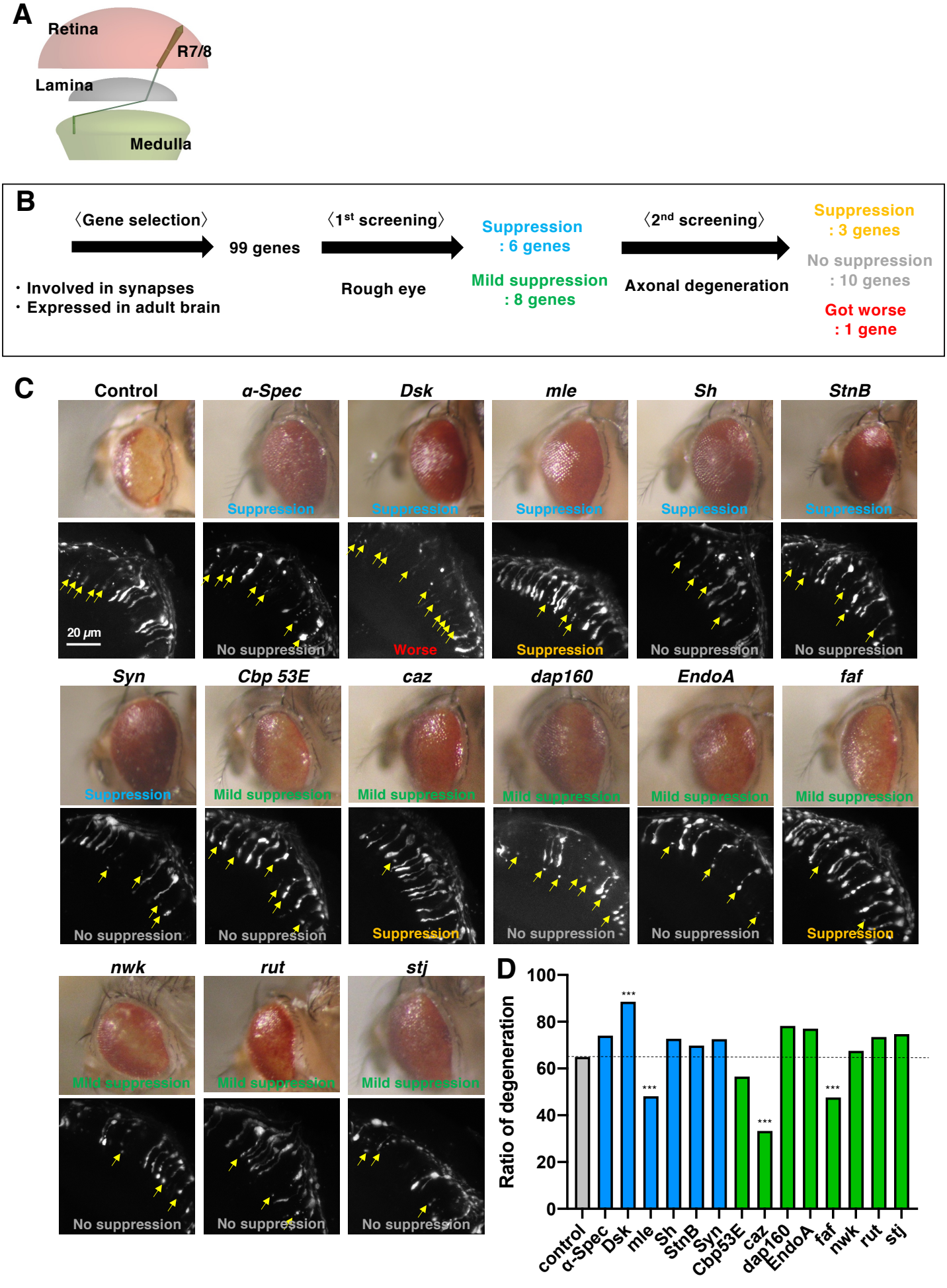

Fig. 1

bioRxiv preprint doi: https://doi.org/10.1101/2021.10.25.465674; this version posted October 26, 2021. The copyright holder for this preprint (which was not certified by peer review) is the author/funder. All rights reserved. No reuse allowed without permission.

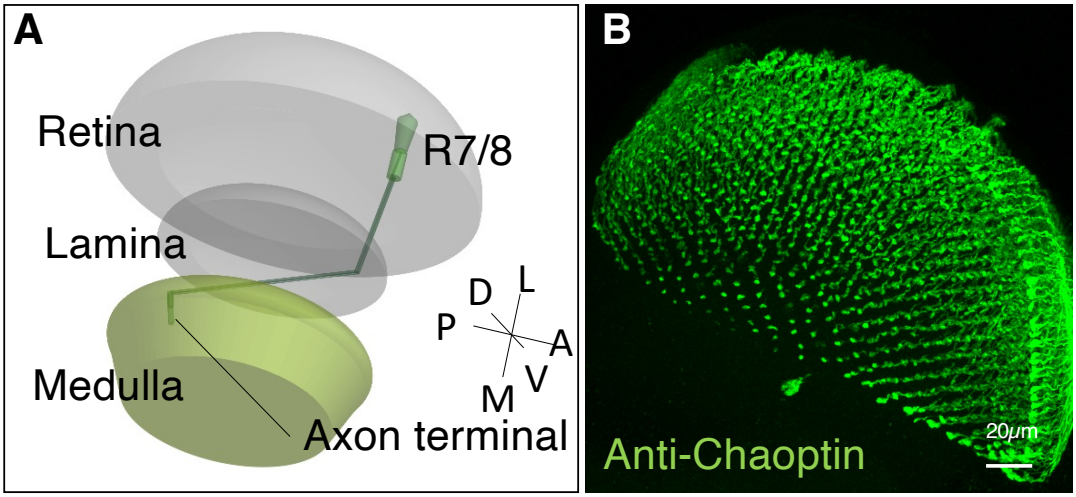

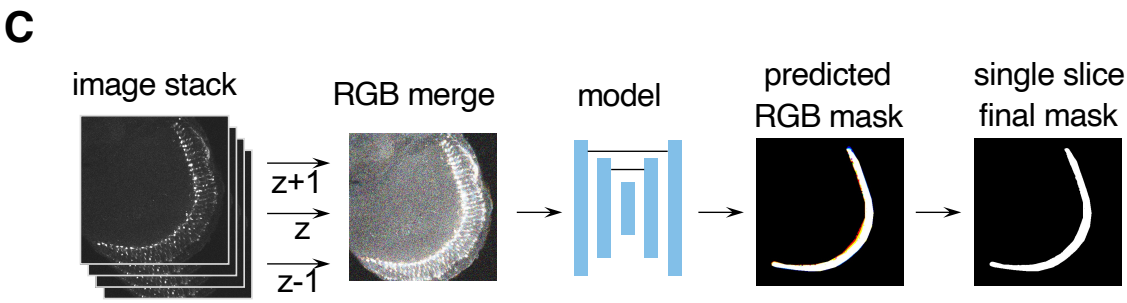

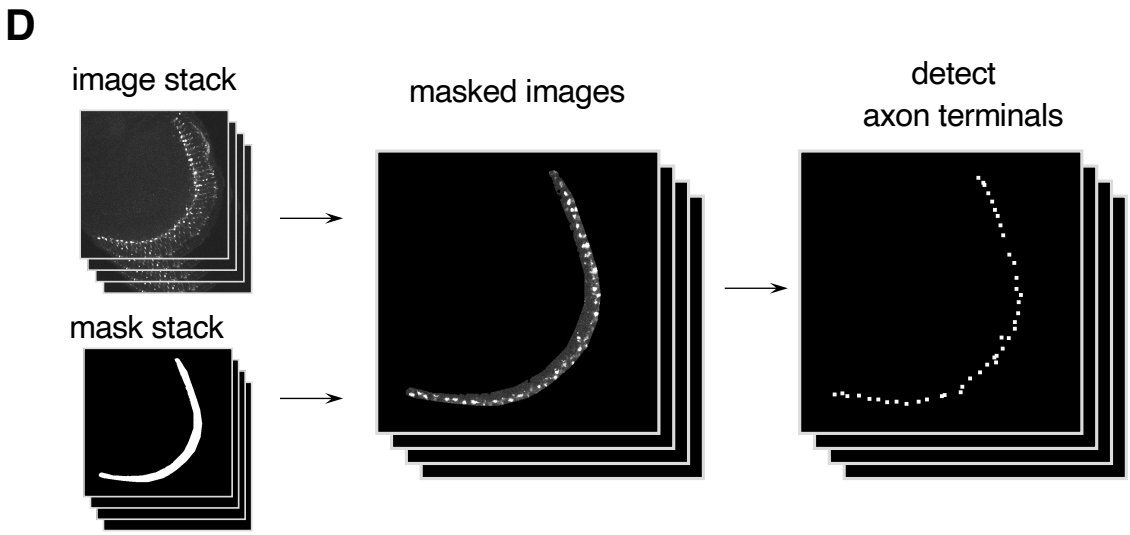

Fig. 2

bioRxiv preprint doi: https://doi.org/10.1101/2021.10.25.465674; this version posted October 26, 2021. The copyright holder for this preprint (which was not certified by peer review) is the author/funder. All rights reserved. No reuse allowed without permission.

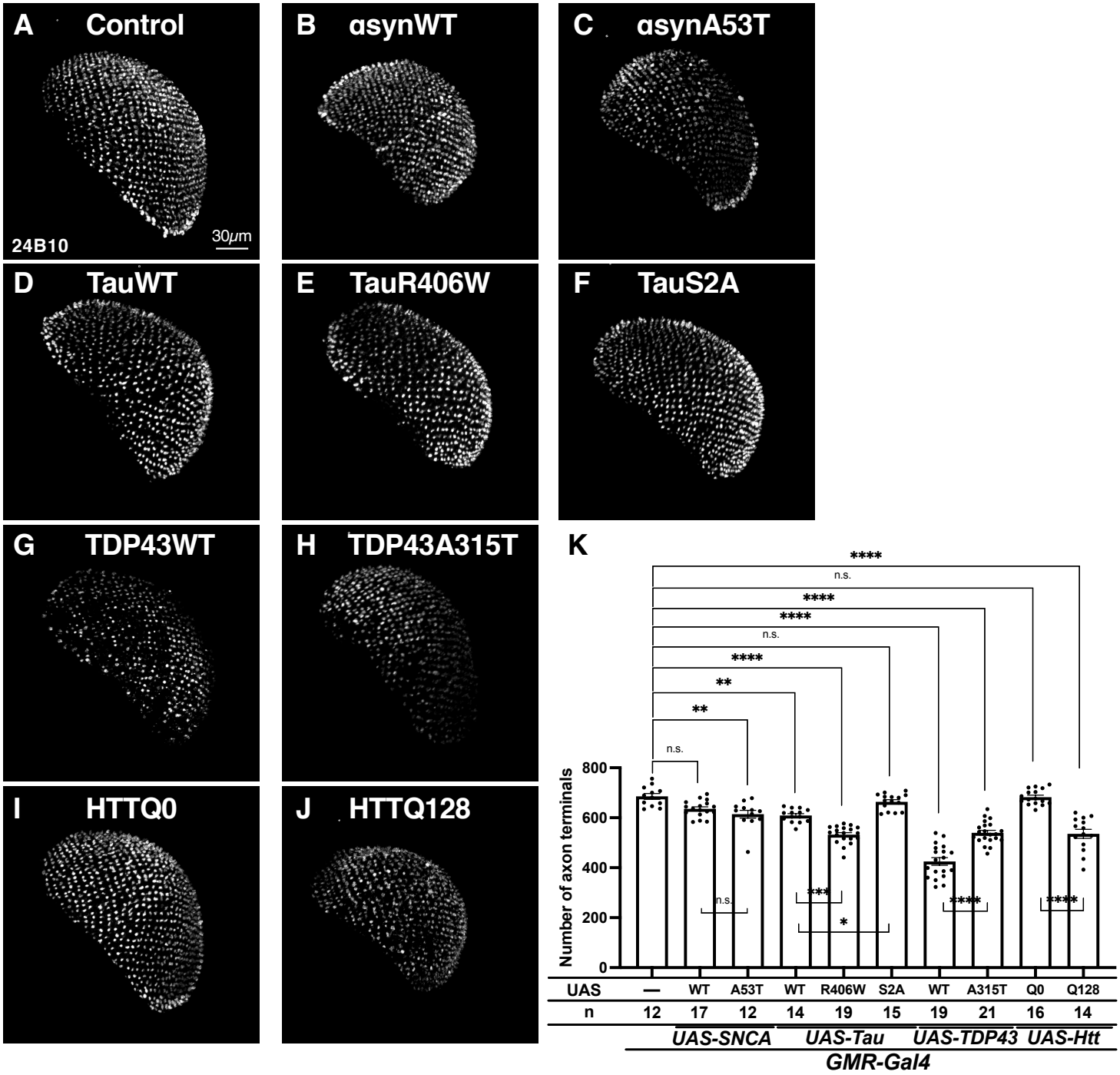

Fig. 3

bioRxiv preprint doi: https://doi.org/10.1101/2021.10.25.465674; this version posted October 26, 2021. The copyright holder for this preprint (which was not certified by peer review) is the author/funder. All rights reserved. No reuse allowed without permission.

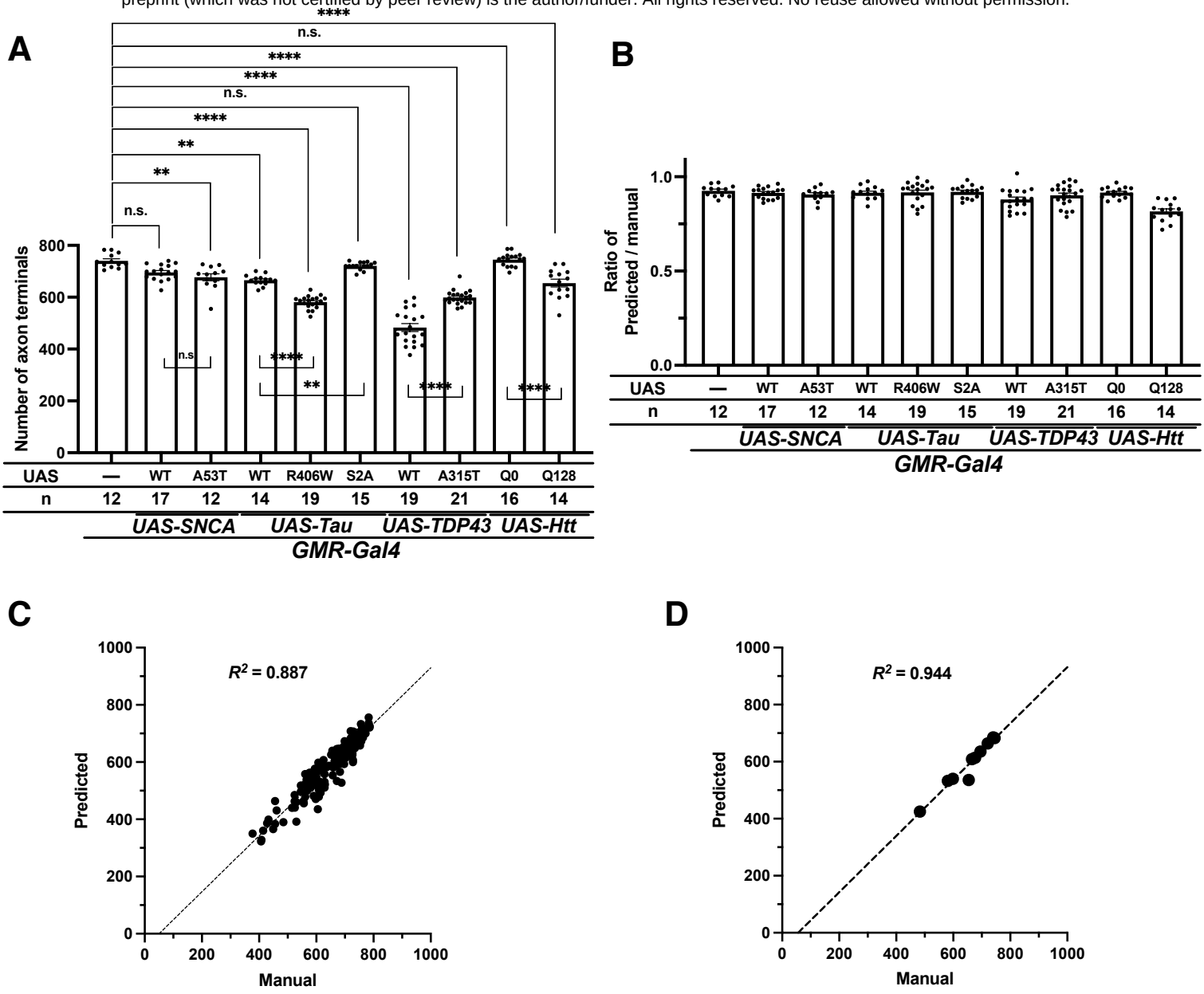

Fig. 4

bioRxiv preprint doi: https://doi.org/10.1101/2021.10.25.465674; this version posted October 26, 2021. The copyright holder for this preprint (which was not certified by peer review) is the author/funder. All rights reserved. No reuse allowed without permission.

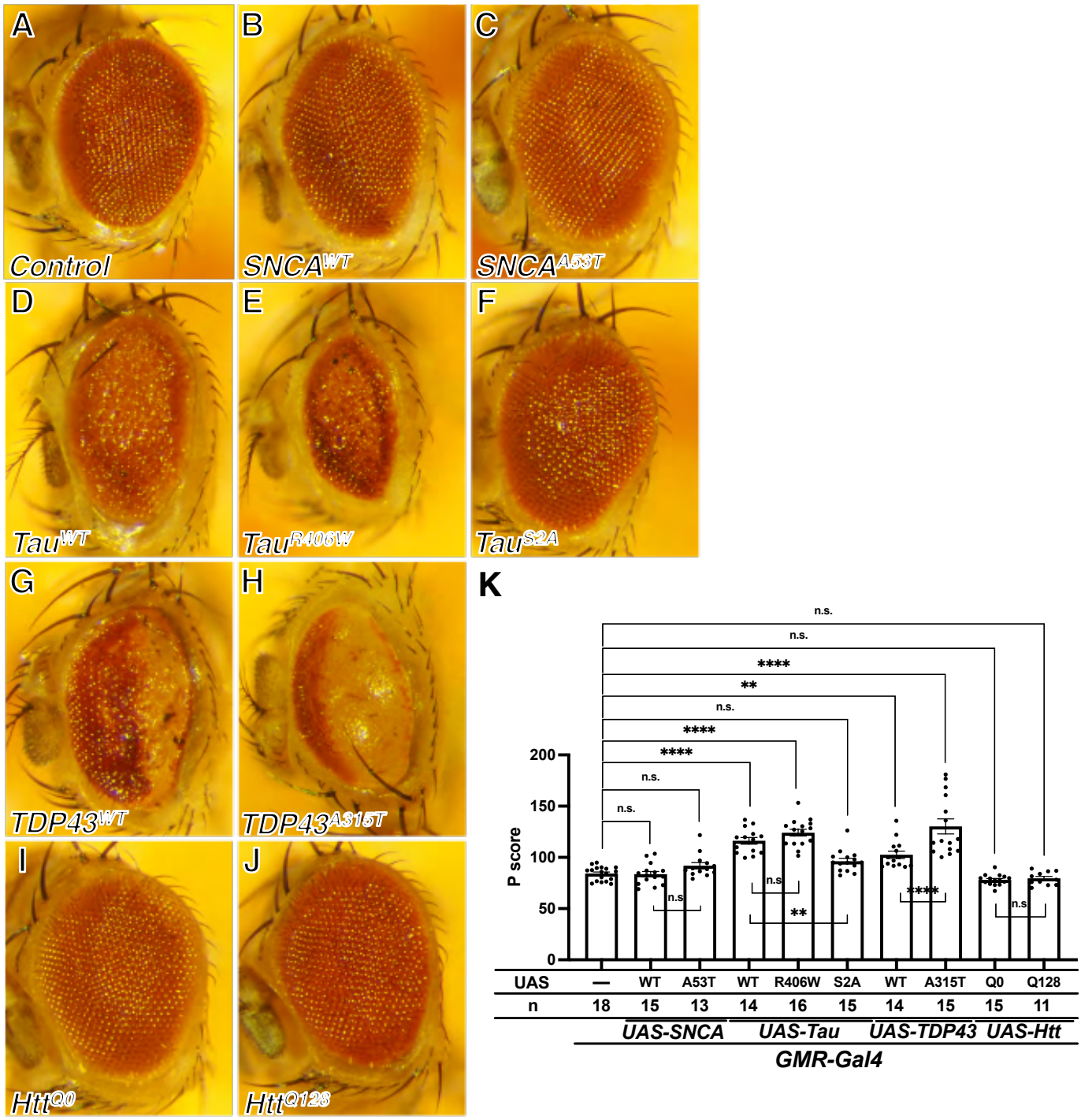

Fig. 5